

# Self-Powered Controllable Transdermal Drug Delivery System

Yuan Yang, Lingling Xu, Dongjie Jiang, Bo Zhi Chen, Ruizeng Luo, Zhuo Liu, Xuecheng Qu, Chan Wang, Yizhu Shan, Yong Cui, Hui Zheng, Zhiwei Wang, Zhong Lin Wang, Xin Dong Guo,\* and Zhou Li\*

Traditional topical ointment applied on the skin surface has poor drug penetration due to the thickening of the stratum corneum for psoriasis. Microneedles (MNs) provide a desirable opportunity to promote drug penetration. However, the common MNs are difficult to meet the requirement of on-demand drug delivery. In this study, a smart electrical responsive MNs is fabricated by introducing conductive material of polypyrrole (PPy). Further, a self-powered controllable transdermal drug delivery system (sc-TDDS) based on piezoelectric nanogenerator (PENG) is developed. The sc-TDDS can control drug release by collecting and converting mechanical energy into electrical energy. The sc-TDDS can release 8.5 ng dexamethasone (Dex) subcutaneously per electrical stimulation. When treating psoriasis-like skin disease with sc-TDDS, the inflammatory skin returned to normal after 5 days, which is obviously better than treating with traditional Dex solution coating. This work provides a promising approach of on-demand transdermal drug release for various disease treatment scenarios.

## 1. Introduction

Psoriasis is a proliferative, chronic inflammatory skin disease with a high incidence, from which 1–3% of people worldwide are suffering.<sup>[1,2]</sup> It presents the symptoms of skin shedding, swelling, itching, inflammatory pain, etc., which makes great inconvenience in the life of patients.<sup>[3,4]</sup> Topical ointment-coating administration is the most common treatment method for skin diseases, but it is reported that only 10–20% or less of drugs could penetrate through the skin.<sup>[5,6]</sup> Besides, the thicker stratum corneum of psoriasis patients makes it more difficult to absorb drugs, which seriously affects the therapeutic effect of ointment.<sup>[7]</sup> As a promising drug delivery method, microneedles (MNs) as minimally invasive devices with the advantages of slight pain, convenient use

Y. Yang, L. L. Xu, D. J. Jiang, R. Z. Luo, X. C. Qu, C. Wang, Y. Z. Shan, Prof. Z. W. Wang, Prof. Z. L. Wang, Prof. Z. Li  
CAS Center for Excellence in Nanoscience, Beijing Key Laboratory of Micro-nano Energy and Sensor  
Beijing Institute of Nanoenergy and Nanosystems  
Chinese Academy of Sciences  
Beijing 101400, China  
E-mail: zli@binn.cas.cn

Y. Yang, L. L. Xu, D. J. Jiang, X. C. Qu, C. Wang, Y. Z. Shan, Prof. Z. W. Wang, Prof. Z. L. Wang, Prof. Z. Li  
School of Nanoscience and Technology  
University of Chinese Academy of Sciences  
Beijing 100049, China

B. Z. Chen, Prof. X. D. Guo  
Beijing Laboratory of Biomedical Materials  
College of Materials Science and Engineering  
Beijing University of Chemical Technology  
Beijing 100029, China  
E-mail: xdguo@buct.edu.cn

R. Z. Luo, Prof. Z. Li  
Center of Nanoenergy Research  
School of Physical Science and Technology  
Guangxi University  
Nanning 530004, China

Dr. Z. Liu  
Beijing Advanced Innovation Centre for Biomedical Engineering  
Key Laboratory for Biomechanics and Mechanobiology  
of Ministry of Education  
School of Biological Science and Medical Engineering  
Beihang University  
Beijing 100191, China

Prof. Y. Cui  
Department of Dermatology  
China-Japan Friendship Hospital  
Beijing 100029, China  
Prof. H. Zheng  
Department of Anesthesiology  
National Cancer Center/National Clinical Research Center  
for Cancer/Cancer Hospital  
Chinese Academy of Medical Sciences and Peking Union  
Medical College  
Beijing 100021, China

Prof. Z. L. Wang  
School of Materials Science and Engineering  
Georgia Institute of Technology  
Atlanta, GA 30332 0245, USA

 The ORCID identification number(s) for the author(s) of this article can be found under <https://doi.org/10.1002/adfm.202104092>.

DOI: 10.1002/adfm.202104092

and high patient compliance provide a great solution, which can penetrate and directly released drug into the epidermis or dermis of skin without obstacles.<sup>[8–10]</sup> For the treatment of psoriasis, MNs can significantly promote the transdermal release efficiency of drugs and improve drug utilization.<sup>[11,12]</sup>

For the treatment of disease, a controlled release system aims to deliver appropriate amount of drug to the target sites at the right time, which could maintain a stable blood drug concentration, reduce adverse reaction and improve utilization of the drug.<sup>[13]</sup> However, the common MNs are difficult to meet on-demand drug delivery requirement of patients, so it is necessary to develop a smart transdermal drug delivery system for controlling drug release.<sup>[14,15]</sup> As an intelligent electro-responsive material, Polypyrrole (PPy) has the superior capability to load and release drugs by switching the oxidative and reductive state. It can be used to incorporate and release anionic,<sup>[16–18]</sup> cationic,<sup>[19]</sup> and neutral drugs.<sup>[20]</sup> For anionic drugs, the principle of loading and release drug of PPy is illustrated in Equation (1). In the oxidative polymerization of PPy, the anionic drugs as dopants are doped into the polymer to balance out positive charges. When PPy was reduced, these anions could leave the polymer as there is a loss of electrostatic attraction between ion and PPy backbone.<sup>[21,22]</sup> PPy drug delivery system with an AC pulsing electrical stimulation has received extensive concern in recent years. PPy presents the alternation of oxidative and reductive state in this pattern, and oxidation and reduction are accompanied by movement of ion and water into and out of the film, resulting in the swelling and shrinking of the polymer, which promotes the diffusion of the drug out of the polymer.<sup>[23,24]</sup>



Considering the source of electrical stimulation energy, nanogenerators including triboelectric nanogenerators (TENG)<sup>[25,26]</sup> and piezoelectric nanogenerators (PENG)<sup>[27,28]</sup> might be a great option. Compared with traditional batteries, the PENG has the following advantage. Firstly, the PENG is light and flexible, which can be easily integrated with drug delivery devices and attach to the skin. Secondly, the materials of PENG are environmental friendliness and good biosafety. Thirdly, PENG collects biomechanical energy (biomechanical motion,<sup>[29,30]</sup> joint bending,<sup>[31]</sup> breathing,<sup>[32]</sup> and heartbeat<sup>[33,34]</sup> etc.) and converts it into electrical energy and without the problem of energy exhaust.<sup>[35,36]</sup> Therefore, there is an opportunity to prepare a self-powered controllable drug delivery system without additional circuit management units, by which the patient can autonomously regulate the amount of drug release.

Here, we fabricated a new conductive MNs by introducing PPy film, further designed and prepared an integrated self-powered controllable drug delivery system (sc-TDDS) based on the piezoelectric nanogenerator (PENG) and the microneedle patch (MNP) for the treatment of psoriasis. Dexamethasone (Dex, an anti-inflammatory drug) loaded MNP is directly connected to the PENG without an additional energy management unit. PENG harvested biomechanical energy to output AC pulse electrical signal by joints bending or hand slapping, and MNP could release Dex in response to electrical stimulation. In this work, we evaluated the working performance of sc-TDDS

in vitro and found that the drug could only be released under electrical stimulation. For each bending of PENG, we recorded that 8.5 ng Dex was released, while there was almost no Dex released when PENG stopped working. In the treatment of psoriasis-like skin disease, the epidermal layer of the psoriasis mouse skin was significantly thinner, and inflammatory factors were reduced after applying the system. These results convincingly demonstrated the system based on PENG and MNP as a lightweight and battery-free device that could achieve on-demand transdermal drug delivery and has a great therapeutic effect for psoriasis.

## 2. Results and Discussion

### 2.1. System Design

We designed a self-powered controllable transdermal drug delivery system (sc-TDDS) based on PENG and MNP (Figure 1a). The system can be applied to any part of the skin, and the patient can control the release and regulate the amount of drug release by bending and slapping the device. PENG of the device harvested and converted biomechanical energy into electrical energy by joints bending or hand slapping and MNP released the drug into skin tissue in response to the electrical signal. The patch contained two MN arrays, polylactic acid-gold-polypyrrole (PLA-Au-PPy) MNs array loading Dex as the working electrode (WE) and polylactic acid-gold (PLA-Au) MNs array as the counter electrode (CE) (Figure 1b). The MNP containing two MN arrays brings three advantages at once: 1) simple for fabrication, the working electrode and the counter electrode were integrated forming, without additional preparation steps. 2) The integrated microneedle patch was more convenient to operate and fix. 3) With the MN structure, the counter electrode could pierce the highly resistive stratum corneum, resulting in significantly reduce the transdermal resistance,<sup>[14]</sup> which is more conducive to release drugs by electrical stimulation. MNP can achieve drug loading and release due to its reversible redox properties of PPy film (Figure 1c). While PPy film was oxidized and deposited, Dex, the anionic drug, was directly doped into the PPy backbone to achieve the drug loading. While PPy film was reduced at a certain voltage, Dex was de-doped from PPy to realize the drug release.

### 2.2. Characterization of the PENG

PENG was composed of polyethylene terephthalate (PET) film, poly(vinylidene fluoride) (PVDF), silver and Kapton film, which serve as the encapsulation layer, the piezoelectric layer, the electrode layer and the substrate layer, respectively. Copper (Cu) tapes were used to attached Cu wires on Ag electrode layers (Figure 2a). The working principle of PENG was illustrated in Figure 2b. At the original state, the electric dipoles in PVDF are arranged along the direction of the two electrodes. When a force is applied to the device in the vertical direction, the polarization charge density increases and creates an electric field, which makes the electrons flow from one end to the other through the external load. When the force was removed,

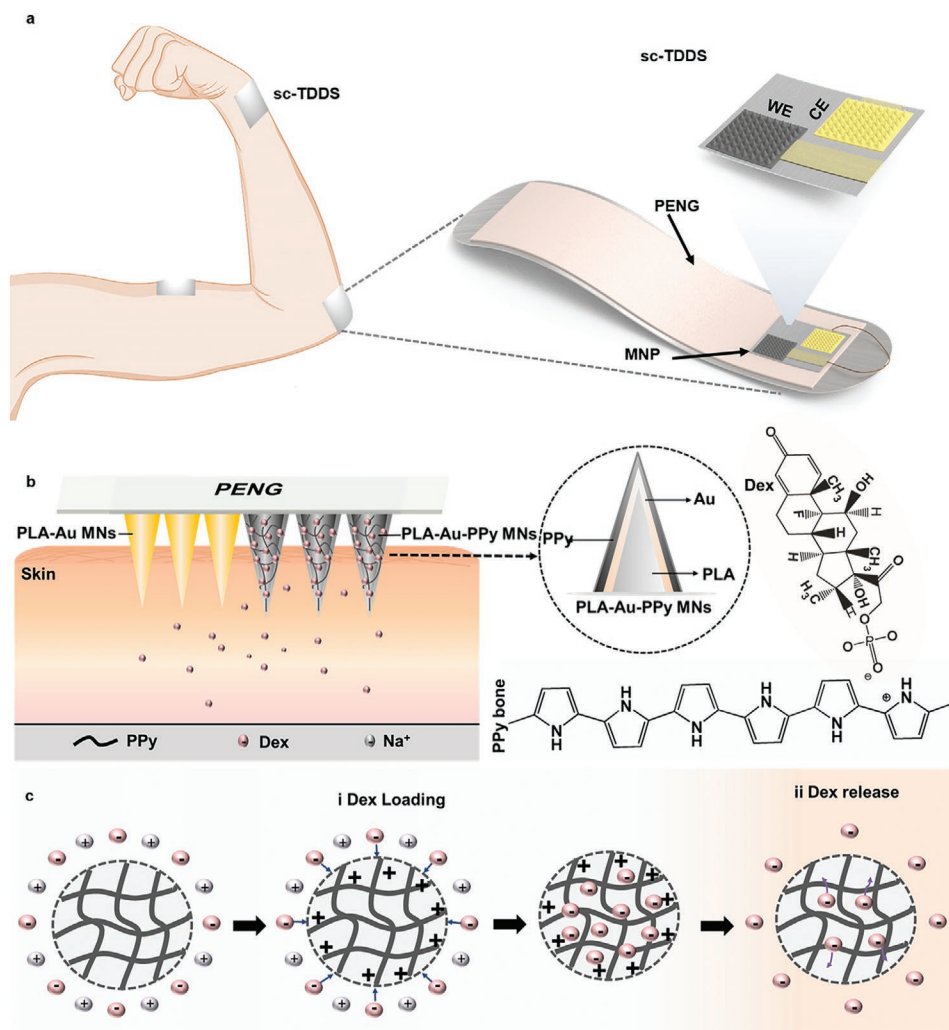


**Figure 1.** Overview of the sc-TDDS. a) sc-TDDS consisted of PENG and MNP; b) MNP including PLA-Au MNs and PLA-Au-PPy MNs loading Dex; c) The mechanism of PPy loading and release Dex. i) Dex was directly doped into the PPy backbone to achieve the drug loading when PPy film was oxidized and deposited. ii) Dex was de-doped from PPy to realize the drug release when PPy film was reduced at a certain voltage.

the electrons would flow in the opposite direction. We used the linear motor to simulate human movement, open-circuit voltage ( $V_{oc}$ ), short-circuit current ( $I_{sc}$ ) and transferred charge ( $Q_{sc}$ ) of PENG were  $\approx 100$  V,  $2 \mu\text{A}$  and  $300$  nC respectively (Figure 2c–e), and the generator had good durability, which can maintain stable output after 100 000 cycles. (Figure S1, Supporting Information). When PENG was attached to the wrist joint, the  $V_{oc}$ ,  $I_{sc}$ , and  $Q_{sc}$  can also reach the 100 V,  $2 \mu\text{A}$  and  $300$  nC (Figure S2a–c and Movie S1, Supporting Information). And When PENG is gently slapped, the output can be easily achieved 50 V,  $1 \mu\text{A}$  and  $100$  nC (Figure S2d–f and Movie S2, Supporting Information).

### 2.3. Fabrication and Characterization of MNP

An MNP containing two different MN arrays, PLA-Au-PPy MN array loading Dex and PLA-Au MN array was fabricated by the thermoforming technology and electrochemical polymerization

(Figure S3, Supporting Information). The morphology of the MNP was presented in Figure 3a. There were two  $10 \times 10$  arrays on a  $15 \times 15$  mm patch, of which the yellow and black parts ( $6 \times 6$  mm) respectively were the PLA-Au MN array and the PLA-Au-PPy MN array. Each MN was conical with a height of  $600 \mu\text{m}$ , a bottom diameter of  $300 \mu\text{m}$  and the needle spacing was  $500 \mu\text{m}$  (Figure 3b,c). The surfaces of PLA-Au MNs were smooth, while the surfaces of PLA-Au-PPy MNs covered with a thin film were relatively rough (Figure S4a, Supporting Information). The mechanical performance of MNs was evaluated by inserting the MNs into a porcine cadaver skin. The bright and fluorescent field image of the pigskin exhibited the MNs created obvious piercing holes on the surface of the skin (Figure 3d). Moreover, the images of the morphology of the PLA-Au-PPy MNs before and after piercing the pigskin showed that PPy film did not break in the process of insertion (Figure S5, Supporting Information). These results demonstrated MNs had strong mechanical properties to completely penetrate the skin and did not leave debris of material in the skin. The thickness

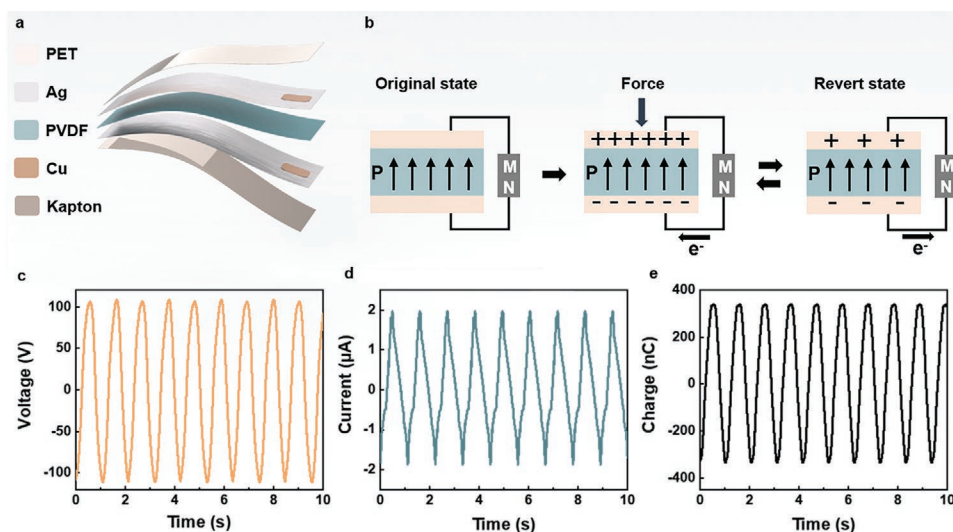


**Figure 2.** Characterization of PENG. a) 3D structure of the PENG including encapsulation layers (PET), piezoelectric layer (PVDF), electrode layer (Ag) and substrate layers (Kapton). b) Working principle of PENG. c–e)  $V_{oc}$ ,  $I_{sc}$ , and  $Q_{sc}$  of the PENG.

of PPy film is the most important factor that affects mechanical performance, electrochemical property and drug loading, which mainly depends on the polymerization charge density. There were the PPy films of PLA-Au-PPy MNs with different polymerization charge densities 300, 400, and 500  $\text{mC cm}^{-2}$ , of which the corresponding thicknesses are  $2 \pm 0.1$ ,  $4 \pm 0.15$ , and  $6 \pm 0.05 \mu\text{m}$ , respectively (Figure S4b,c, Supporting Information), demonstrating PPy film thickness was linearly related to polymerization charge density (Figure 3e). The force-displacement curves of MNs presented that the applied force increases

with the displacement, and the slopes of PLA-Au-PPy MNs and PLA-Au MNs were greater than PLA MNs, indicating that the gold layer and PPy film can enhance the mechanical property of MN and the mechanical strength of MN increased with the thickening of PPy film (Figure S6, Supporting Information). Further, we measured the electrochemical performance of PLA-Au-PPy MNs. Electrochemical impedance spectroscopy (EIS) was used to investigate the conductivity of the PLA-Au-MNs (Figure 3f). The impedance of PLA-Au-PPy MN array with the polymerization charge of 300, 400, and 500  $\text{mC cm}^{-2}$  were 956,

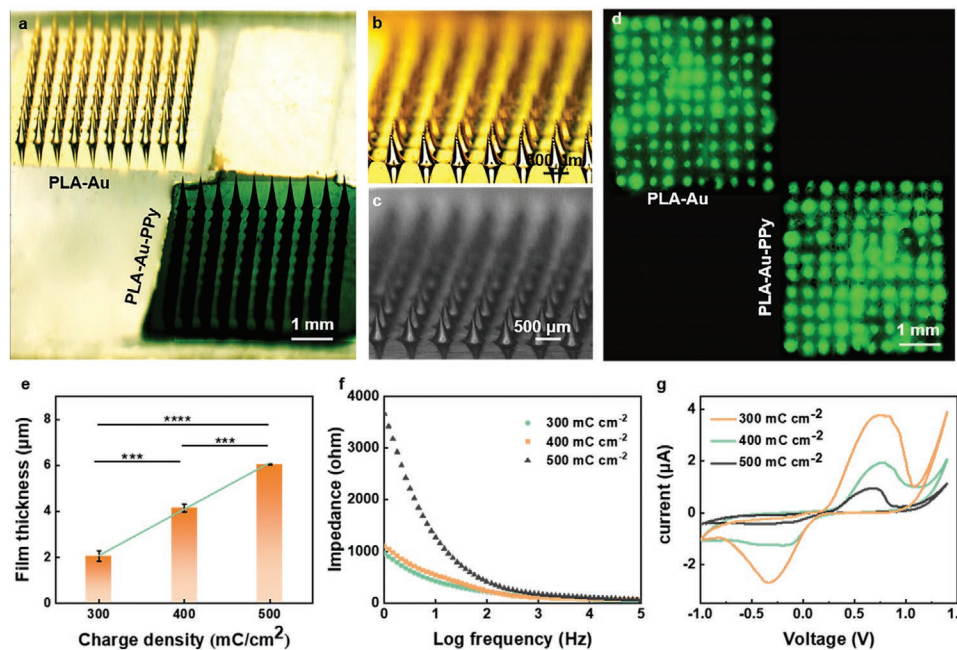


**Figure 3.** Performance characterization of MNs. a–c) Brightfield micrographs of the patch containing PLA-Au and PLA-Au-PPy MNs arrays. d) The fluorescent images of porcine skin after application of the MNP. e) The thickness of PPy film of PLA-Au-PPy MNs. f,g) EIS and CV curve of PLA-Pt-PPy MNs. Means  $\pm$  SD,  $N = 5$ ,  $*P < 0.05$ ,  $**P < 0.01$ ,  $****P < 0.0001$ . ns, no significance.

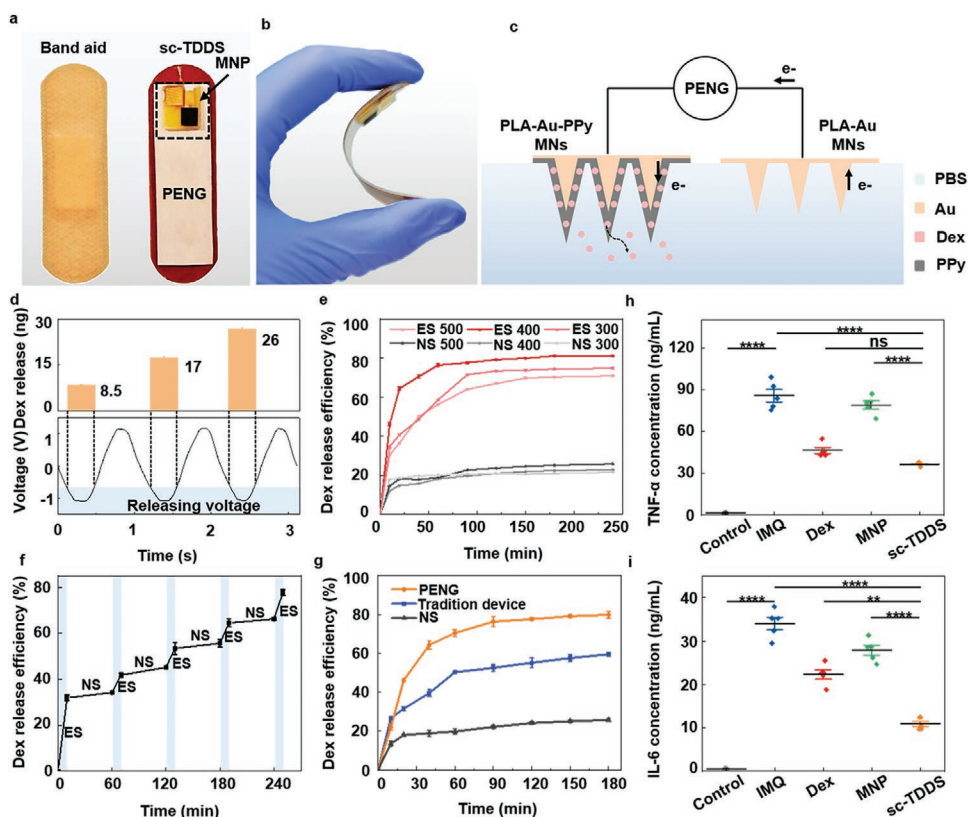


**Figure 4.** Drug delivery in vitro. a) Comparison photograph of sc-TDDS and commercial band-aid. b) Photograph of sc-TDDS in the bending state. c) Schematic circuit diagram of sc-TDDS release drug in PBS. d) Dex release amount and corresponding Dex release trigger cosine waveform e) Dex release efficiency with PENG (electrical stimulation (ES) and no stimulation (NS)). f) Dex release efficiency from the MNP by intermittent driving PENG (ES for 10 min and NS for 50 min). g) Dex release efficiency with PENG and traditional device, no stimulation as the control group. h,i) TNF- $\alpha$  and IL-6 concentration in LPS-induced RAW 264.7 cells pre-treated with Dex solution, MNP and sc-TDDS. Means  $\pm$  SD,  $N = 5$ ,  $*P < 0.05$ ,  $**P < 0.01$ ,  $****P < 0.0001$ . ns, no significance.

1108, and 3666  $\Omega$  in 1 Hz matching the frequency of the human motion, indicating the impedance of PPy film increase with the film thickness.<sup>[37]</sup> Cyclic voltammetry (CV) was applied to explore the redox behavior of PLA-Au-PPy MNs. As shown in Figure 3g. The MNs had an oxidation peak at about +0.8 V and a reduction peak at about -0.34 V which was an indicator of Dex release.

#### 2.4. sc-TDDS Integration

An integrated sc-TDDS was assembled by sticking MNP to the surface of PENG, and two arrays of MNP were connected to the two electrode layers of PENG using copper wire. The overall size of the device was  $7.5 \times 3.5$  cm same as commercial band-aids (Figure 4a), and a total weight of only 1.5 g (Figure S7a, Supporting Information). The system was light and flexible (Figure 4b), which can be easily attached to the skin.

#### 2.5. Drug Delivery In Vitro

The Dex loading and release kinetics of the system was investigated in 0.01 mol L<sup>-1</sup> PBS. The circuit diagram of sc-TDDS was

shown in Figure 4c, PENG outputted AC electrical signal and PPy backbone obtained electron, leading to Dex de-doped and diffused into PBS solution to realize drug release. The amount of Dex loaded in PLA-Pt-PPy MNs with the polymerization density 300, 400, and 500 mC cm<sup>-2</sup> were measured to be  $45 \pm 4.6$ ,  $89 \pm 1.2$ , and  $129 \pm 1.4$  ng per needle (Figure S7b, Supporting Information). The experimental results indicated that the higher the polymer charge density, the more anionic drugs doped into the PPy film. The output signals of the voltage applied on the two MN array, loop current and transfer charge were sine waves and the peak values were about 1 V and 2  $\mu$ A, respectively (Figure S8a,b, Supporting Information). The negative voltage (-0.34 V) of pulse electrical signal was utilized to trigger drug release and per pulse stimulation could release  $8.5 \pm 0.25$  ng (Figure 4d). For the release efficiency of Dex from the MNP, in the absence of electrical stimulation, only 10–20% drug diffused into the PBS solution from the surface of the PLA-Au-PPy MNs. Nevertheless, under the action of electrical stimulation, 70–80% Dex could be released (Figure 4e). In the process of drug release, PPy film continuously transforms between oxidation and reduction states under pulse electrical stimulation, and PPy may doped with other anions in PBS. With most of the Dex released, the previously doped anions may give priority to de-doping when PPy film is reduced, which

makes it difficult for the remaining Dex to be released in the short term. Among them, PLA-Au-PPy MNs with the charge density of  $500 \text{ mC cm}^{-2}$  had a lower drug release efficiency, because the MNs had thicker PPy film and higher impedance. The process of Dex release is that the anions break away from PPy backbone and diffused from the inner part of the film to the surface and then, to the buffer solution. So that, the thicker PPy film will hinder the drug de-doping and diffusion.<sup>[38]</sup> Considering the drug loading and drug release kinetics of sc-TDDS, the polymerization density of  $400 \text{ mC cm}^{-2}$  is the optimal parameter for the fabrication of MNP. MNP with a polymerization density of  $400 \text{ mC cm}^{-2}$  was used in the next study.

Drug release efficiency of MNP could be controlled by PENG (Figure 4f). When PENG was driven to produce electrical energy for stimulating the MNP, a linear release profile of Dex was obtained, and when PENG stopped working, almost no Dex was released from the MNP. Meanwhile, compared with the traditional device, the sc-TDDS has a higher drug release efficiency after 10 min (Figure 4g). The reasons could be that: When a constant voltage was applied, the conductivity of PPy film would gradually decrease due to the loss of doped ions, which would reduce the drug release rate.<sup>[39]</sup> While under pulsed electrical stimulation, PPy film continuously transforms between oxidation and reduction states, which maintains the conductivity of PPy film and promotes the diffusion of drugs, resulting in higher drug release efficiency.<sup>[37]</sup> Further, we explored the biocompatibility of the microneedle materials and the anti-inflammatory activity of Dex released from the MNP with RAW 2674 cells in vitro. The results showed that the viability of the cells was above 85% (Figure S8c, Supporting Information), and the concentration of the pro-inflammatory mediators IL-6 and TNF- $\alpha$  induced by LPS was obviously decreased after treatment with Dex from the sc-TDDS (Figure 4h,i). These results suggested that MNP has good biocompatibility and the drug retain its bioactivity during the electric-stimulated release process.

## 2.6. Psoriasis Treatment In Vivo

To visualize the release process of drugs in vivo, we loaded sodium fluorescein (Flu) instead of Dex into the PPy film for drug release in vivo. The MNs were pierced into the skin of Sprague Dawley (SD) rats, and Flu was released by electrical stimulation from PENG or a commercial battery. The pulse voltage and current from PENG applied on a rat were typically about 1.5 V and 2  $\mu\text{A}$ . The voltage and current applied by traditional battery were 1.5 V and 24  $\mu\text{A}$  under the same conditions (Figure S9a,b, Supporting Information). The release process of Flu was monitored and imaged using an in-vivo imaging system (IVIS) spectrum. The result showed compared with the no electrical group, there was a 5 times stronger fluorescent signal in penetration sites of sc-TDDS group. It indicating that sc-TDDS could achieve controlled drug release in vivo. The current generated by the PENG is smaller than the traditional batteries (1.5 V battery) but has a higher drug release efficiency under AC pulse electrical signals, which is particularly suitable for controlling the release of unstable drugs. (Figure S9c,d, Supporting Information).

Furthermore, the sc-TDDS was applied to treat psoriasis with BALB/c mice as the animal model. Following a week of continuous psoriasis-like modeling using imiquimod (IMQ), mice with successful modeling showed thickened cuticle, erythema and scales, significantly reduced body weight, and enlarged spleen (Figure S10a–c, Supporting Information). Histological changes of psoriasis are characterized by hyperproliferation and poor differentiation of epidermal keratinocytes, increased skin vascularization and leukocyte infiltration, which can be counted by Baker scores.<sup>[40]</sup> The changes of inflammatory factors in the blood and inflammatory-related cells in spleen are also important indicators.

After successful modeling, psoriasis mice were treated using sc-TDDS, MNP without electrical stimulation and Dex solution containing same the amount of drug as MNP (Figure 5a). MNP could create indelible puncturing sites on the skin surface and penetration cavities ( $\approx 500 \mu\text{m}$ ) inside the epidermis layer of the mouse skin (Figure 5b), confirming that the MNs can well penetrate and completely released Dex into skin tissue. In the treatment of psoriasis-like disease, the weight and ear thickness of mice in the treatment group (sc-TDDS) has gradually been normal after 5 days, compared to the other treatment groups (Dex and MNP) (Figure S11a,b, Supporting Information).

Skin histopathology is the most intuitive evaluation criterion for psoriasis. The skins of each group were collected after the mice were sacrificed on the fifth day. As shown in the hematoxylin/eosin (H&E) staining picture (Figure 5c). Compared with IMQ group, the epidermis layer thickness of sc-TDDS treatment group was significantly thinner, and the Baker score of the back skin decreased significantly (Figure S12, Supporting Information), which was close to the skin thickness of the control group (Figure 5d). A significant treatment effect for psoriasis was also reflected on the mouse ear which showed that Dex was absorbed by tissues and play a systemic anti-inflammatory effect (Figure S13, Supporting information). The concentration of the pro-inflammatory mediators IL-6 and TNF- $\alpha$  in blood was obviously reduced after treatment with sc-TDDS (Figure 5e,f and Figure S14 Supporting Information). While the sizes of the spleen become smaller with the splenic congestion was significantly reduced (Figure S15, Supporting Information). We further investigated the inflammatory cells in the spleen, and the results showed that the IMQ would lead to a decrease of CD4<sup>+</sup> T cells and an increase of CD11c<sup>+</sup> cells. After treatment of sc-TDDS group, the percentage of CD4<sup>+</sup> T cells increased and the percentage of CD11c<sup>+</sup> cells decreased, which was closer to that of the control group. The reason may be that Dex reduced the inflammation of spleen.<sup>[41]</sup> (Figure 5g and Figures S16 and S17, Supporting Information). In the process of treatment, the therapeutic effects of the Dex and MNP groups were not obvious, because in Dex solution group, only a little drug could penetrate the skin, and in MNP treatment group, only 10–20% Dex from the surface of MNP were directly released into skin without electrical stimulation. These results indicated that the Dex doped into the PPy film of the MNP was released in vivo by bending PENG, and sc-TDDS could directly release drugs into skin tissues and achieve controlled drug release in vivo, which has high drug utilization and good therapeutic effects.

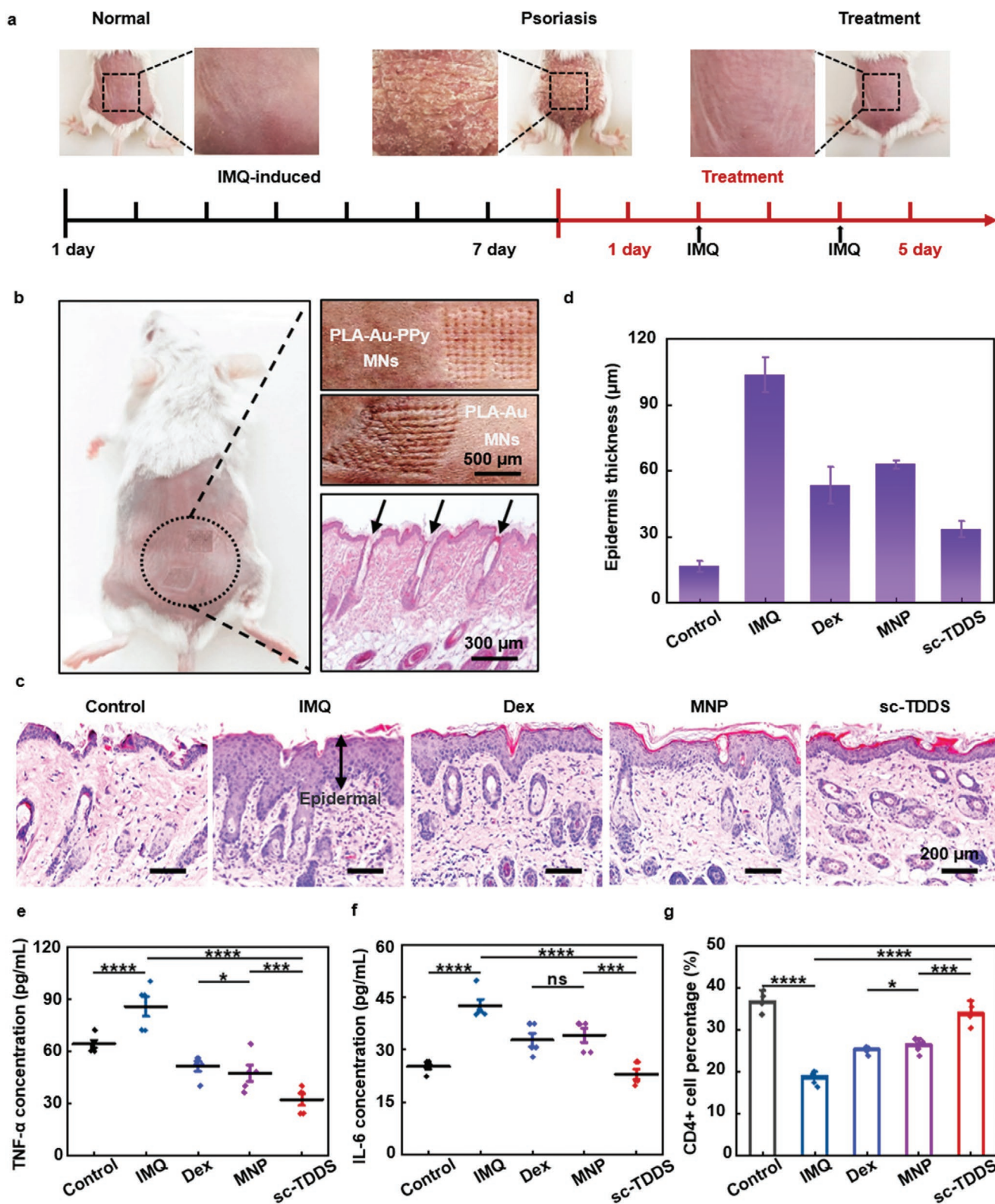


**Figure 5.** Psoriasis treatment. a) The timeline and the corresponding photograph of the psoriasis model and treatment process. b) Mouse skin after treatment with MNP and its corresponding histological section (bottom right). c) H&E staining of mouse skin induced by IMQ and treated with Dex solution, MNP and sc-TDDS, normal skin as the control group. d) Epidermis thickness measured from HE staining picture. e, f) TNF- $\alpha$  and IL-6 concentration of mouse induced by IMQ and treated with Dex solution, MNP and sc-TDDS, normal mice as the control group. g) Statistical analysis of the percentage of CD4<sup>+</sup> T cells from the mouse spleen. Means  $\pm$  SD,  $N = 5$ , \* $P < 0.05$ , \*\* $P < 0.01$ , \*\*\*\* $P < 0.0001$ . ns, no significance.

### 3. Conclusion

In this work, we have fabricated a two-electrodes conductive MNP by introducing PPy film, and developed an integrated sc-TDDS based on PENG and MNP. The system could collect and convert biomechanical energy from human movement into electrical energy to control drug release on demand and presented a good therapeutic effect in the treatment of psoriasis. MNP has higher efficiency of the drug release under AC pulsed electrical stimulation from PENG and the current in this system for drug release is lower than commercial batteries, which can better maintain the activity of drugs. The device has the advantages of slight pain, lightweight, flexible, on-demand drug delivery and high drug utilization. The system can serve as a general device to effectively deliver drugs for the treatment of arthritis, mental and analgesia etc. Furthermore, this system can be combined with a biomolecular detection system to form a closed-loop self-powered diagnosis and treatment system in the future.

### 4. Experimental Section

**Materials:** Polydimethylsiloxane (PDMS, Sylgard 184) was purchased from Dow Corning (Midland, USA). Polylactic acid (PLA) particles were obtained from Lakeshore Biomaterials Inc. (AL, USA). Pyrrole (Py, 98%) was received from Beijing Ilex Technology Co., Ltd. (Beijing, China). Dexamethasone sodium phosphate (Dex), Sodium fluorescein (Flu), lipopolysaccharide and TNF- $\alpha$  and IL-6 ELISA kits were purchased from Beijing Solaibao Technology Co., Ltd (Beijing, China). FITC-labeled anti-CD4 mAb was obtained from Sigma-Aldrich (MO, USA). Female SD mice and BALB/c mice were purchased from the Institute of Laboratory Animal Sciences (Beijing, China).

**Fabrication of PENG:** The PENG consisted of piezoelectric layer, electrode layer, encapsulation layer and a flexible substrate layer. PVDF film (3 $\times$ 6 cm) coated the silver on both sides was utilized as piezoelectric layer, and the layers of silver were especially employed as electrodes. The copper wires were fixed on the silver electrode layers. The ultrathin PET film and Kapton film were introduced as the package layer and flexible substrate layer, respectively. All parts were stucked together layer by layer.

**Characterization of PENG:** The PENG was driven by a linear motor (frequency, 1 Hz, operating distance, 50 mm; acceleration, 1 m s<sup>-2</sup>; deceleration, 1 m s<sup>-2</sup>; maximum speed, 1 m s<sup>-1</sup>). The electrical signals (voltage, current, and transferred charge) were recorded by the oscilloscope.

**Fabrication of MNP:** The MNP containing different matrix materials was fabricated by three step process. Initially, the supporting polylactic acid (PLA) MNP including two 10 $\times$ 10 MN arrays was first prepared using hot pressure method based on a polydimethylsiloxane (PDMS) mold, of which the height was 600  $\mu$ m, the basal diameter was 300  $\mu$ m, and the space distance between MNs was 500  $\mu$ m. Next, polylactic acid-gold (PLA-Au) MNP containing two Au coated MN arrays were obtained by sputtering a layer of gold on the PLA MNP covered some mask. Finally, one of two PLA-Au MN arrays as the working electrode (WE), polylactic acid-gold-polypyrrole (PLA-Au-PPy) MN array was carried out at room temperature in a three electrodes cell with electrochemical workstation, a platinum (Pt) plate (1 cm<sup>2</sup>) as the counter electrode (CE) and a saturated calomel electrode (SCE) as the reference electrode (RE). The electrolyte was an aqueous solution containing 0.1 mol L<sup>-1</sup> pyrrole (Py) and 0.02 mol L<sup>-1</sup> dexamethasone sodium (Dex). The Dex-doped PPy films were performed on the exposed surface of the working electrode (PLA-Au MNs) by applying a constant voltage of 0.8 V with the charge density 300, 400, and 500 mC cm<sup>-2</sup> to receive PLA-Au-PPy MNs. There were two different MNs arrays, PLA-Au MN array and PLA-Au-PPy MN array on a patch. The patch was rinsed with de-ionized water for

removing the unreacted Py monomer and Dex and dried in the vacuum oven.

**Characterization of MNP:** The bright field images were carried out with a stereomicroscope (SZX7, Olympus, Japan) for recording the morphology of MNs. A cold field emission scanning electron microscope (SEM, SU8020) was used to observe the surface morphology of the MNs and the thickness of PPy film. To further evaluate the insertion capability of MNs with different structures, the MNP was inserted into the hairless pigskin with a force of 10 N, and gently peeled off after 2 min. To facilitate the observation the rate of insertion, 10  $\mu$ L, 1  $\times$  10<sup>-3</sup> M fluorescein sodium (Flu) was dropped on the insertion site, keeping for 1 min, and taken away. The insertion sites on the skin were exposed under a stereomicroscope (SZX7, Olympus, Japan).

A dynamometer (Force Gauge Model, Mark-10, USA) was used to measure the mechanical properties of the MNs. The mechanical sensor moved down to the horizontal platform at a speed of 0.5 mm min<sup>-1</sup> until a preset maximum load (20 N) was reached. Cyclic voltammetry (CV) and electrochemical impedance spectroscopy (EIS) were introduced to test the electrochemical performance of PLA-Au-PPy MNs using the electrochemical station (ES, CHI660e). CV with the scanning voltage of -1 to 1.5 V at the scan rate of 1 V s<sup>-1</sup> and EIS between 1 and 10<sup>5</sup> Hz was carried out in 0.01 mol L<sup>-1</sup> phosphate buffer solution (PBS) (pH = 7.2).

**Drug Delivery In Vitro:** To determine the loading Dex capacity of PLA-Au-PPy MNs, Dex release was carried out by using an electrochemical station (ES) applying cycle voltammetry (CV) with the range of -1 to 1 V and the scan rate 1 V s<sup>-1</sup> for 10 000 cycles to promote the release of all drug into 1 mL, 0.01 mol L<sup>-1</sup> PBS. The amount of released Dex was quantified by the UV absorbance at 242 nm (the characteristic peak of Dex) using ultraviolet spectrophotometer. To observe the release kinetics of Dex from sc-TDDS, Dex release from PLA-Au-PPy MN array with the polymerization charge density of 300, 400, 500 mC cm<sup>-2</sup> were performed in 1 mL 0.01 mol L<sup>-1</sup> PBS. The two MN arrays of the MNP were respectively connected to the two electrodes of PENG which was driven by motor, and the group without electrical stimulation was used as a control. The Dex release efficiency was determined by the percentage of cumulative drug release and drug loading. Meanwhile, the electrode signals including the voltage across two MNs arrays, the loop current and transferred charge were recorded by an oscilloscope. To achieve on-demand drug release, PENG was intermittently driven by linear motor to power the MNP (electrical stimulation for 10 min, no stimulation for 50 min).

**The Bioactivity of Released Dex:** To evaluate the bioactivity of Dex released from the MN patch, RAW264.7 cells were next plated in 24-well plates at a density of 1.0  $\times$  10<sup>4</sup> cells per well and cultured in high glucose Dulbecco's modified Eagles medium (DMEM) containing 10% fetal bovine serum and 1% penicillin-streptomycin at 37 °C with 5% CO<sub>2</sub>. Cells were next treated with Dex solution (1  $\mu$ g mL<sup>-1</sup>), Dex solution (diluting 10 times to produce the same concentration as Dex solution) from sc-TDDS and MNP followed stimulated with 1  $\mu$ g mL<sup>-1</sup> lipopolysaccharide (LPS) for 24 h. The standard indirect quantitative ELISA kits were used to determine the concentration of the inflammatory factor TNF- $\alpha$  and IL-6 in supernatants. Meanwhile, cytotoxicity of relevant material of the MNP and LPS was analyzed by 3-(4, 5-dimethylthiazol-2-yl)-2, 5-diphenyltetrazolium bromide (MTT) assay.

**Drug Delivery In Vivo:** To visualize the drug release in vivo, Fluorescein sodium (Flu), as anion dopant, instead of Dex was loaded into the PLA-Au-PPy MN array. The Flu loaded MNP was pierced into the back skin without the hair of female SD rats (200 $\pm$ 10 g). Rats were divided into three groups and severally treated with MNP (without electrical stimulation), MNP electrically stimulated by 1.5 V battery and the sc-TDDS (MNP electrical stimulated by the PENG which was driven by motor with the same output in vitro experiment) for 1, 2, and 3 h. Next, the rats were imaged using in vivo imaging system (IVIS, Xenogen 200, Caliper Life Sciences, Hopkinton, MA) to measure the fluorescent intensity of Flu on the insertion area and analyzed the Flu release efficiency in vivo.

**Psoriasis Modeling Process:** Twenty-five BALB/c mice (6–8 weeks), of which the back hair (2 $\times$ 2 cm) was removed, were randomly divided into

five groups (each group containing five rats). One of the groups served as a blank control group, and other mice were used to model psoriasis. The depilation area on the back and right ear of the mouse were applied 5% imiquimod (IMQ) cream evenly on the depilatory area at a dose of 50 mg cm<sup>2</sup>, once a day for 7 days.

**The Treatment Process of Psoriasis:** Except for the model group mice (IMQ), the remaining three groups of mice were severally treated with Dex solution (100 μL, 0.1 mg mL<sup>-1</sup>), the MNP (without electrical stimulation) and the sc-TDDS (MNP electrical stimulated by the PENG which was driven by motor with the same output in vitro experiment) for 2 h. After the mice were sacrificed, the treatment area skins were removed and stored in tissue fixative at 4 °C. The skins were stained with H&E for observing the skin appearance and analyzing the infiltration of inflammatory cells. The spleens were removed and masked to measure the CD4<sup>+</sup> and CD11c<sup>+</sup> inflammatory cells by flow cytometry. Blood was extracted by removing the eyeball followed the centrifugal separation to obtain the serum, in which the inflammatory factors (TNF-α and IL-6) were tested by the standard ELISA kit. The animal experiments were approved by Committee on Ethics of Beijing Institute of Nanoenergy and Nanosystems (A-2019027).

**Statistical Analysis:** All results were performed with the simple size of  $n \geq 3$ . The statistics were expressed as the mean values  $\pm$  SD (standard deviation). An ordinary one-way ANOVA was used to calculate the *P*-values. Differences with  $P < 0.05$ ,  $P < 0.01$ ,  $P < 0.001$ ,  $P < 0.0001$ , and not significant were considered statistically significant and were labeled with \*, \*\*, \*\*\*, \*\*\*\*, and ns, respectively, Origin 8.0 was used for statistical analysis.

## Supporting Information

Supporting Information is available from the Wiley Online Library or from the author.

## Acknowledgements

Y.Y. and L.L.X. contributed equally to this work. This work was financially supported by the Beijing Natural Science Foundation (JQ20038), the National Natural Science Foundation of China (61875015, 51873015, 81970994), China Postdoctoral Science Foundation (2020M680302), Key-Area Research and Development Program of Guangdong Province (2018B030331001), the Joint Project of BRC-BC (Biomedical Translational Engineering Research Center of BUCT-CJFH) (XK2020-05) and the Fundamental Research Funds for the Central Universities.

## Conflict of Interest

The authors declare no conflict of interest.

## Data Availability Statement

Research data are not shared.

## Keywords

conductive microneedles, drug delivery, on-demand, psoriasis, self-powered

Received: April 30, 2021  
Published online:

- [1] J. E. Greb, A. M. Goldminz, J. T. Elder, M. G. Lebwahl, D. D. Gladman, J. J. Wu, N. N. Mehta, A. Y. Finlay, A. B. Gottlieb, *Nat. Rev. Dis. Primers* **2016**, 2, 16082.
- [2] M. Sticherling, *Autoimmun. Rev.* **2016**, 15, 1167.
- [3] A. W. Armstrong, A. R. Ford, C. J. Chambers, E. Maverakis, C. A. Dunnick, M. M. Chren, J. M. Gelfand, C. M. Gibbons, B. M. Gibbons, C. J. Lane, *J. Invest. Dermatol.* **2019**, 139, 1037.
- [4] A. Rendon, K. Schäkel, *Int. J. Mol. Sci.* **2019**, 20, 1475.
- [5] M. R. Prausnitz, R. Langer, *Nat. Biotechnol.* **2008**, 26, 1261.
- [6] A. W. Armstrong, C. Read, *JAMA* **2020**, 323, 1945.
- [7] A. Mitra, Y. Wu, *Expert Opin. Drug Delivery* **2010**, 7, 977.
- [8] Z. Z. Zhang, Z. Z. Zi, E. E. Lee, J. W. Zhao, D. C. Contreras, A. P. South, E. D. Abel, B. F. Chong, T. Vandergriff, G. A. Hosler, P. E. Scherer, M. Mettlen, J. C. Rathmell, R. J. DeBardinis, R. C. Wang, *Nat. Med.* **2018**, 24, 617.
- [9] W. Li, R. N. Terry, J. Tang, M. R. Feng, S. P. Schwendeman, M. R. Prausnitz, *Nat. Biomed. Eng.* **2019**, 3, 220.
- [10] G. S. Liu, Y. F. Kong, Y. S. Wang, Y. H. Luo, X. D. Fan, X. Xie, B. R. Yang, M. X. Wu, *Biomaterials* **2020**, 232, 119740.
- [11] H. Y. Du, P. Liu, J. J. Zhu, J. J. Lan, Y. Li, L. B. Zhang, J. T. Zhu, J. Tao, *ACS Appl. Mater. Interfaces* **2019**, 11, 43588.
- [12] Z. H. Zhao, Y. D. Chen, Y. L. Shi, *RSC Adv.* **2020**, 10, 14040.
- [13] S. T. Sanjay, W. Zhou, M. Dou, H. Tavakoli, L. Ma, F. Xu, X. J. Li, *Adv. Drug Delivery Rev.* **2018**, 128, 3.
- [14] S. Kusama, K. Sato, Y. Matsui, N. Kimura, H. Abe, S. Yoshida, M. Nishizawa, *Nat. Commun.* **2021**, 12, 658.
- [15] J. B. Yang, Y. J. Li, R. Ye, Y. Zheng, X. L. Li, Y. Z. Chen, X. Xie, L. L. Jiang, *Microsyst. Nanoeng.* **2020**, 6, 112.
- [16] Q. H. Cui, T.-H. Le, Y.-J. Lin, Y.-B. Miao, I.-T. Sung, W.-B. Tsai, H.-Y. Chan, Z.-H. Lin, H.-W. Sung, *Nano Energy* **2019**, 66, 104120.
- [17] Z. J. Du, G. Q. Bi, X. T. Cui, *Adv. Funct. Mater.* **2018**, 28, 12.
- [18] Q. L. Ouyanga, X. L. Feng, S. Y. Kuang, N. Panwara, P. Y. Song, C. B. Yang, G. Yang, X. Y. Hemui, G. Zhang, H. S. Yoon, J. P. Tam, B. Liedberg, G. Zhu, K.-T. Yong, Z. L. Wang, *Nano Energy* **2019**, 62, 610.
- [19] H.-N. Niloufar, S. Devleena, A. Yassan, J. P. Annes, R. N. Zare, *Nanoscale* **2017**, 9, 143.
- [20] D. Samanta, N. Hosseini-Nassab, A. D. McCarty, R. N. Zare, *Nanoscale* **2018**, 10, 9773.
- [21] D. Svirskis, J. Travas-Sejdic, A. Rodgers, S. Garg, *J. Controlled Release* **2010**, 146, 6.
- [22] A. Puiggali-Jou, L. J. del Valle, C. Aleman, *J. Controlled Release* **2019**, 309, 244.
- [23] C. Boehler, F. Oberueber, M. Asplund, *J. Controlled Release* **2019**, 304, 173.
- [24] Q. Q. Zhang, J. X. Kang, Z. Q. Xie, X. G. Diao, Z. Y. Liu, J. Zhai, *Adv. Mater.* **2018**, 30, 1703323.
- [25] F.-R. Fan, Z.-Q. Tian, Z. L. Wang, *Nano Energy* **2012**, 1, 328.
- [26] H. Y. Zou, L. T. Guo, H. Xue, Y. Zhang, X. F. Shen, X. T. Liu, P. H. Wang, X. He, G. Z. Dai, P. Jiang, H. W. Zheng, B. B. Zhang, C. Xu, Z. L. Wang, *Nat. Commun.* **2020**, 11, 2093.
- [27] K. Dong, X. Peng, Z. L. Wang, *Adv. Mater.* **2020**, 32, 1902549.
- [28] Z. Liu, L. L. Xu, Q. Zheng, Y. Kang, B. J. Shi, D. J. Jiang, H. Li, X. C. Qu, Y. B. Fan, Z. L. Wang, Z. Li, *ACS Nano* **2020**, 14, 8074.
- [29] D. J. Jiang, X. C. Qu, H. Ouyang, B. J. Shi, Y. Zou, S. Y. Chao, Y. B. Fan, Z. Li, *InfoMat* **2020**, 2, 1191.
- [30] G. X. Liu, S. H. Xu, Y. Y. Liu, Y. Y. Gao, T. Tong, Y. C. Qi, C. Zhang, *Adv. Funct. Mater.* **2020**, 30, 1909886.
- [31] W. Tang, J. J. Tian, Q. Zheng, L. Yan, J. X. Wang, Z. Li, Z. L. Wang, *ACS Nano* **2015**, 9, 7867.
- [32] Q. Zheng, B. J. Shi, F. R. Fan, X. X. Wang, L. Yan, W. W. Yuan, S. H. Wang, H. Liu, Z. Li, Z. L. Wang, *Adv. Mater.* **2014**, 26, 5851.
- [33] H. Ouyang, Z. Liu, N. Li, B. J. Shi, Y. Zou, F. Xie, Y. Ma, Z. Li, H. Li, Q. Zheng, X. C. Qu, Y. B. Fan, Z. L. Wang, H. Zhang, Z. Li, *Nat. Commun.* **2019**, 10, 1821.

- [34] Q. Zheng, Q. Z. Tang, Z. L. Wang, Z. Li, *Nat. Rev. Cardiol.* **2021**, *18*, 7.
- [35] J. Wang, S. M. Li, F. Yi, Y. L. Zi, J. Lin, X. F. Wang, Y. L. Xu, Z. L. Wang, *Nat. Commun.* **2016**, *7*, 12744.
- [36] R. Hinchet, H.-J. Yoon, H. J. Ryu, M.-K. Kim, E.-K. Choi, D.-S. Kim, S.-W. Kim, *Science* **2019**, *365*, 491.
- [37] V. Alarautalahti, M. Hiltunen, N. Onnela, S. Nymark, M. Kellomaki, J. Hyttinen, *Biomaterials* **2018**, *106*, 2202.
- [38] K. M. Woeppel, X. S. Zheng, Z. M. Schulte, N. L. Rosi, X. T. Cui, *Adv. Healthcare Mater.* **2019**, *8*, 1900622.
- [39] B. Alshammary, F. C. Walsh, P. Herrasti, C. Ponce de Leon, *J. Solid State Electrochem.* **2016**, *20*, 839.
- [40] H. X. Yan, W. W. Li, Y. Zhang, X. W. Wei, L. X. Fu, G. B. Shen, T. Yin, X. Y. Li, H. S. Shi, Y. Wan, Q. Y. Zhang, J. Li, S. Y. Yang, Y. Q. Wei, *Immunol. Res.* **2014**, *60*, 112.
- [41] F. Liu, S. P. Wang, B. Liu, Y. K. Wang, *Cells* **2020**, *9*, 511.